Mild Hydrothermal Syntheses and Thermal Behaviors of Hydrogarnets $Sr_3M_2(OH)_{12}$ (M = Cr, Fe, and Al)

Guangshe Li,[†] Shouhua Feng,*[,†] Liping Li,[‡] Xirong Li,[†] and Weijie Jin[†]

Key Laboratory of Inorganic Hydrothermal Synthesis and Department of Chemistry, Jilin University, Changchun 130023, P. R. China, and Department of Physics, Jilin University, Changchun 130023, P. R. China

Received April 17, 1997. Revised Manuscript Received August 19, 1997[⊗]

Hydrogarnets $Sr_3M_2(OH)_{12}$ (M = Cr, Fe, and Al) were synthesized from mild hydrothermal systems at 240 °C with $Sr(OH)_2{\cdot}8H_2O$, $Cr(NO_3)_3{\cdot}9H_2O$, $Fe(NO_3)_3{\cdot}9H_2O$, and $Al(OH)_3$ as the starting materials. High solubility of the input species and basic concentration in the reaction systems considerably lower crystallization temperatures and enhance the crystallinity of the resulting hydrogarnets. The structural stability and thermal properties of Sr based hydrogarnets were investigated by X-ray diffraction, DTA-TG, infrared, and X-ray photoelectron spectroscopies. With increasing temperature, Sr based hydrogarnets underwent fast dehydration due to the loss of the nearest OH^- species of Sr−OH dodecahedra. During the course of decomposition, valence variations of the hydrogarnet framework ions, e.g., Fe and Cr directly determined the decomposition process and phase compositions in final decomposition products. The decomposition product of $Sr_3Cr_2(OH)_{12}$ in air was a mixture of $SrCrO_4$ and SrO, but in N_2, a mixture of a rhombohedral phase $Sr_4Cr_2O_8$ with some amorphous phase was observed; in either O_2 or N_2, $Sr_3Fe_2(OH)_{12}$ decomposed to an unknown phase, which was not a perovskite $Sr_3Fe_2O_{7-x}$. $Sr_3Al_2(OH)_{12}$ decomposed to a single phase $Sr_3Al_2O_6$. In Sr−Fe hydrogarnet, two different symmetric octahedra of $Fe(OH)_6$ were revealed by Mossbauer spectroscopy. Mild hydrothermal crystallization and the thermal decomposition behaviors of Sr-based hydrogarnets are discussed.

Introduction

Garnet structural materials are most important due to their potential applications. For example, yttrium aluminum garnet (YAG) and yttrium iron garnet (YIG) are well-known important laser and magnetic materials. The pressure-induced behavior studies of such structures have been reported.[1] The structures of most garnets are iso-structural with the so-called "grossulars": $Ca_3Al_2Si_3O_{12}$. When each silicon ion in the formula is replaced by four protons, "hydrogrossulars" or "hydrogarnet" $Ca_3Al_2(OH)_{12}$ can be formed.[2] The structural characteristic of the point vacancy is most interesting, and the properties of such defect type garnets differ from those of traditional garnets due to the difference in coordination states of framework atoms in both lattices.

Hydrogarnets have been synthesized by various preparative methods including aging of precipitated gels and sol−gels processes,[3] hydrolysis of complex oxides,[4] and a high temperature−pressure hydrothermal method.[5] Each of these methods has its own limitation. For example, the high temperature−pressure hydrothermal method is complicated and has strict pressure conditions; for the other preparative methods mentioned above, firing is an essential crystallization step, which usually results in particle agglomerates.[6] Mild hydrothermal synthesis below 240 °C and under homogeneous pressure has been a promising route for preparing novel inorganic compounds.[7] In hydrothermal systems, various initial reaction compositions may result in new structures and certain valence characteristics by homogeneous reaction and valence control of reactant elements under a hydrostatic pressure.[8,9] In addition, the structural and physical properties vary with the preparation condition and defect properties.[10]

The positions of protons in the hydrogarnet lattice are difficult to determine due to the very small atomic weight of proton. The structures of some hydrogarnets had been examined by neutron diffraction and X-ray diffraction methods.[11] A typical example is $Ca_3Al_2(OD)_{12}$, in which slightly distorted tetrahedra of oxygen atoms surrounded by more distorted deuterium tetra-

* To whom correspondence should be addressed.
[†] Key Laboratory.
[‡] Department of Physics.
[⊗] Abstract published in *Advance ACS Abstracts,* October 1, 1997.

(1) (a) Shimada, M. *Jpn. J. Appl. Phys.* **1972**, *11*, 964. (b) Liu, L.-G., *Science* **1977**, *195*, 990. (c) Ohtani, E.; Irifune, T.; Fujino, K. *Nature* **1981**, *294*, 62.
(2) Hyde, B. G. *Inorganic crystal structures*; John Wiley & Sons: New York, 1989.
(3) (a) Ito, J.; Frondel, C. *Am. Mineral.* **1967**, *52*, 1105. (b) Ito, J. *Mater. Res. Bull.* **1968**, *3*, 495.
(4) Kwestroo, W.; Van Gerven, H. C. A.; Van Hal, H. A. M. *Mater. Res. Bull.* **1977**, *12*, 161.
(5) Moran-Miguelez, E.; Alario-Franco M. A.; Joubert, J. C. *Mater. Res. Bull.* **1986**, *21*, 107.
(6) Kriechbaum, G. W.; Kleinschmit, P. *Angew. Chem. Adv. Mater.* **1989**, *101*, 1446.
(7) (a) Feng S.; Greenblatt, M. *Chem. Mater.* **1992**, *4*, 388. (b) An, Y.; Feng, S.; Xu, Y.; Xu, R. *Chem. Mater.* **1996**, *8*, 356. (c) Zhao, C.; Feng, S.; Chao, Z.; Shi, C.; Xu, R.; Ni, J., *J. Chem. Soc., Chem. Commun.* **1996**, 1641. (d) Xu, Y.; Feng, S.; Pang, W., *J. Chem. Soc., Chem. Commun.* **1996**, 1305.
(8) Li, G.; Feng, S.; Li, L. *J. Solid State Chem.* **1996**, *126*, 74.
(9) Barrer, R. M., *Hydrothermal Chemistry of Zeolites*; Academic Press Inc.: New York, 1982.
(10) (a) Li, G.; Li, L.; Zhao, M. *Phys. Status Solidi B* **1996**, *197*, 165. (b) Arashi, H.; Naito, H.; Nakata, M. *Solid State Ionics* **1995**, *76*, 313.
(11) Dennis, W.; Foreman, J. R. *J. Chem. Phys.* **1968**, *48*, 3037.

S0897-4756(97)00237-8 CCC: $14.00

hedra were shown. Mossbauer spectroscopy is a more effective method in detecting the coordination states and electronic states of Fe ions, it is especially sensitive to the local environment.[12] However, to our knowledge, there are no reports on the Mossbauer study of the hydrogarnet structural materials to date.

In this paper, we report the syntheses of the hydrogarnets, $Sr_3M_2(OH)_{12}$ (M = Cr, Fe, and Al), from mild hydrothermal systems, their structural characteristics and stability as well as thermal decomposition behaviors. The coordination states of Fe ions in Sr−Fe hydrogarnet are examined by Mossbauer spectroscopy.

Experimental Section

$Sr(OH)_2{\cdot}8H_2O$ (A.R.), $Cr(NO_3)_3{\cdot}9H_2O$ (A.R.), $Fe(NO_3)_3{\cdot}9H_2O$ (A.R.), and $Al(OH)_3$ (A.R.) were used as the starting materials in the syntheses, and NaOH was employed as a mineralizer. The molar ratios of the initial compositions were $2.0-1.0SrO:0.5M_2O_3:3.0-1.5Na_2O:600H_2O$ (M = Cr, Fe, and Al). The typical synthetic procedure for $Sr_3Cr_2(OH)_{12}$ is described as follows. $Cr(NO_3)_3{\cdot}9H_2O$ (1.2 g) was first dissolved in 30 mL of distilled water to form a solution, to which 0.8 g of $Sr(OH)_2{\cdot}8H_2O$ was added with magnetic stirring. NaOH (3 M) solution was dropwise added to adjust the pH of the reaction mixture to 13−14. The mixture was then sealed in a Teflon-lined stainless steel autoclave with a filling capacity of 75% and allowed to crystallize at 240 °C for 3 days; the synthetic procedure for $Sr_3Al_2(OH)_{12}$ is a little more complex because of the low solubility of $Al(OH)_3$ in water and its increased solubility in basic system. Blue (from Cr system), brown (Fe system), and white (Al system) crystalline powders were filtered, washed with distilled water until pH = 7, and dried at room temperature.

The phases of all powder products were identified by means of X-ray diffraction (XRD) on a Rigaku, D/max-γA, 12 kW diffractometer with a rotating target and Ni-filtered Cu Kα radiation at room temperature. Silicon powder (99.999% purity) was used as an internal standard for peak position determination. The raw data were also corrected for background and 2θ with a Program STEPCO of XRS-82 system.[13] The lattice parameters of the products were refined by least-squares methods.

The morphologies of the products were observed by Electron microscopy (H-8100IV transition electron microscope (TEM)) under an accelerated voltage of 200 kV. Particles of the samples to be measured were directly deposited onto Formvar-coated copper grids and air-dried before the examination.

The compositions of the products were determined by inductively coupled plasma (ICP) with a Perkin-Elmer plasma 40 emission spectrometer. Simultaneous differential thermal analysis and thermogravimetric (DTA-TG) curves were recorded on a PE-DTA 1700-TGA7 PC thermoanalyzer in air or in flowing O_2 (or N_2) at a heating rate of 10 °C/min. Performing the measurements under different atmospheres ensured the different thermal decomposition behaviors of the hydrogarnets. The furnace was cooled to room temperature at a rate of ca. 25 °C/min. The fresh decomposition products of the Sr based hydrogarnets in DTA-TG measurements were also examined by XRD. The infrared (IR) spectra were recorded on a Nicolet 5DX IR spectrometer on samples pelletized with KBr powder.

Valence states were determined by X-ray photoelectron spectroscopy (XPS). The XPS for powder samples fixed on double sided tapes was measured on an ESCA-LAB MKII X-ray photoelectron spectrometer from VG Co. with Al Kα radiation, and the base pressure was 10^{-7} Pa. The C1s signal was used to correct the charge effects.

^{57}Fe Mossbauer spectra were recorded at room temperature by an Oxford MS-500 constant acceleration spectrometer. The velocity was calibrated with an α-Fe foil. The radiation source was ^{57}Co/Rh. The thickness of the absorber used in the measurements was 3−5 mg of Fe/cm^2.

Results and Discussion

1. Mild Hydrothermal Synthesis and Characterization of $Sr_3M_2(OH)_{12}$. Hydrothermal crystallization is a relatively complex process because many factors are involved, such as the initial reactants, the ratio of reaction components, concentration, pH, reaction time, crystallization temperature, and pressure. Besides the effect of OH^- concentration, the reactivities of the starting materials determine directly the crystallization temperatures.[14]

The synthesis and characterization of nanocrystalline $Sr_3Cr_2(OH)_{12}$ are emphasized in our study. $Cr(NO_3)_3{\cdot}9H_2O$ and $Sr(OH)_2{\cdot}8H_2O$ are suitable starting materials for the synthesis of $Sr_3Cr_2(OH)_{12}$. This is because the solubility of $Cr(NO_3)_3{\cdot}9H_2O$ in water is high and that of $Sr(OH)_2{\cdot}8H_2O$ increases with temperature. When NaOH solution was added into Cr(III) salt solution, an amphoteric slurry, $Cr_2O_3{\cdot}nH_2O$, with light blue color was produced. This slurry, under hydrothermal conditions, can be crystallized to various products, e.g., γ-CrO(OH), $Na_3[Cr(OH)_6]{\cdot}xH_2O$, $NaCrO_2$, and $NaCr_n(OH)_{3n+1}{\cdot}xH_2O$ by using different concentrations of NaOH.[15] In our hydrothermal system, although the crystallization mechanism may be complicated, the formation reaction of $Sr_3Cr_2(OH)_{12}$ can be proposed as follows:

$$3Sr(OH)_2 + Cr_2O_3{\cdot}nH_2O = Sr_3Cr_2(OH)_{12} + (n-3)H_2O$$

The effect of the concentration of OH^- on the formation reaction was investigated by adjusting the NaOH concentration of the reaction system. When the pH of the reaction systems is lower than 7, no solid product was obtained, even though the initial molar ratio of Sr/Cr is equal to 1.5; in a pH range, 7−8, certain amorphous phases with no obvious diffraction peaks appeared; the hydrogarnet phase began to crystallize at pH > 8, and its crystallinity increased with increase of pH. These showed that the hydrothermal crystallization for single-phase $Sr_3Cr_2(OH)_{12}$ demanded a high concentration of OH^-. The crystallinity of the resulting product is gradually enhanced by increasing the OH^- concentration, which may be ascribed to the consumption of hydroxyl species in the formation reaction of the hydrogarnet lattice and in lowering the crystallization temperature. As the pH was fixed as 14, initial molar ratios of Sr/Cr around the ideal ratio, 1.5, led to a single-phase product, whereas the ratio of Sr/Cr deviating greatly from the ideal ratio gave poorly crystalline products, as detected by XRD.

Figure 1a shows XRD pattern for the single phase product in the Sr−Cr hydrogarnet system at room temperature. The phase was well indexed in cubic symmetry. Systematic absences gave a space group,

(12) Ebsworth, E. A. V.; Rankin, D. W. H.; Cradock, S. *Structural Methods in Inorganic Chemistry*; Blackwell Scientific Publishers: Cambridge, MA, 1987.

(13) Baerlocher, Ch. *The X-ray Rietveld System*; Inst. Fur Kristallographie & Petrographie der ETH: Zurich, 1982.

(14) (a) Dutta, P. K.; Asiaie, R.; Akbar, A. A.; Zhu, W. *Chem. Mater.* **1994**, *6*, 1542. (b) Asiaie, R.; Zhu, W.; Akbar, S. A.; Dutta, P. K. *Chem. Mater.* **1996**, *8*, 226.

(15) Chekhomova, L. F.; Sereda, B. P.; Smirnov, S. V.; Tyurin, Yu. N.; Berg, N. A. *Izv, Akad. Nauk SSSR, Neorg. Mater.* **1991**, *27*, 1256.

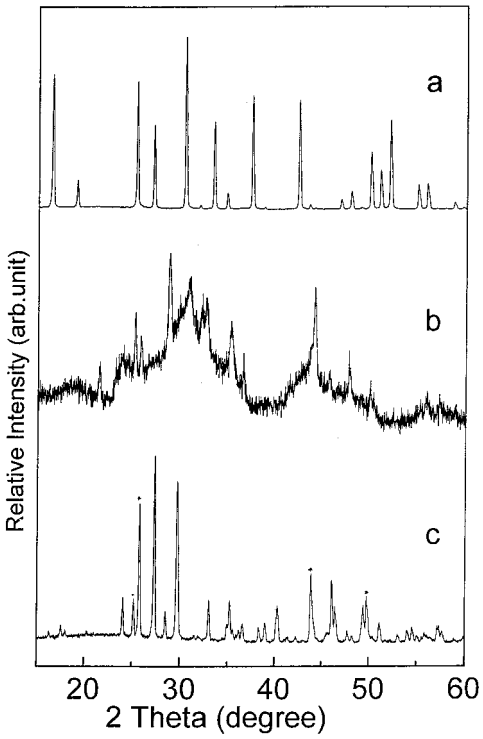

Figure 1. XRD patterns for (a) $Sr_3Cr_2(OH)_{12}$ crystallized in cubic symmetry (*Ia*3*d*) from mild hydrothermal system, (b) the sample obtained by decomposition of Sr−Cr hydrogarnet in DTA-TG measurement at 750 °C in flowing N_2, where $Sr_4Cr_2O_8$ coexisted with certain amorphous phases, and (c) the sample (mixture of $SrCrO_4$ and $SrCO_3$), produced by heating Sr−Cr hydrogarnet at 1150 °C in air; asterisks denote the diffraction peaks of $SrCO_3$.

*Ia*3*d*, which showed that the sample was iso-structural with the hydrogarnet $Sr_3Sc_2O_6{\cdot}6H_2O$.[16] The cell parameter is $a = 13.144(1)$ nm. Figure 2a shows TEM morphology of the product. All particles are within nanometer scale (<50 nm) and have two grain shapes: needles and platelets. This implies two different crystallization habits. Compositional analysis of the product measured by ICP corresponds to a molar ratio of Sr/Cr, 1.5. Figure 3a gives IR spectra at room temperature for the sample. A sharp band at $\nu \approx 3600$ cm^{-1} was observed, characteristic of hydroxyl OH^- species, suggested by Nakamoto.[17] A broad band at 3150−3550 cm^{-1} was attributed to a trace of surface adsorbed water. Gato et al.[18] investigated exchange of water and heavy water in hydrogarnets and found that, the IR spectra for both $Ca(OH)_2$ and hydrogarnet $3CaO{\cdot}Al_2O_3{\cdot}6H_2O$ were characterized by the OH^- stretching band at ca. 3600 cm^{-1}. The characteristic band at $\nu \approx 3600$ cm^{-1} of the sample is thus ascribed to the existence of hydroxyl groups in the hydrogarnet lattice. Figure 4 shows the surface XPS of Cr2p (see solid line) in the product. The binding energies of $Cr2p_{3/2}$ and $Cr2p_{1/2}$ in the product are 577.1 and 585.3 eV, respectively, which suggests only trivalent Cr ions in the product. Therefore, the formula for the single-phase product can be written as $Sr_3Cr_2(OH)_{12}$.

(16) McLune, W. F., Ed. *Powder Diffraction File: Inorganic Phases*; JCPDS International Centre for Powder Diffraction Data: Swarthmore, PA, Card No. 24-1186, 1989.

(17) Nakamoto, K. *Infrared and Raman Spectra of Inorganic and Coordinaion Compounds*, 4th ed.; John, Wiley & Sons: New York, 1986.

(18) Goto, S.; Ueki, Y.; Yasumura, N. *Ceram. Trans.* **1994**, *40*, 115.

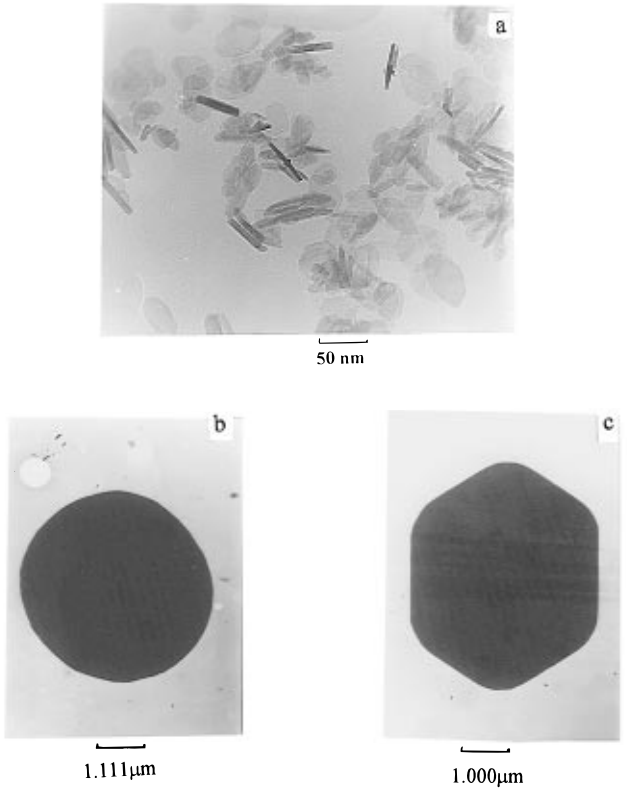

Figure 2. TEM photographs for (a) $Sr_3Cr_2(OH)_{12}$, with particles of size <50 nm, having two grain shapes, needles and platelets, (b) $Sr_3Fe_2(OH)_{12}$, and (c) $Sr_3Al_2(OH)_{12}$.

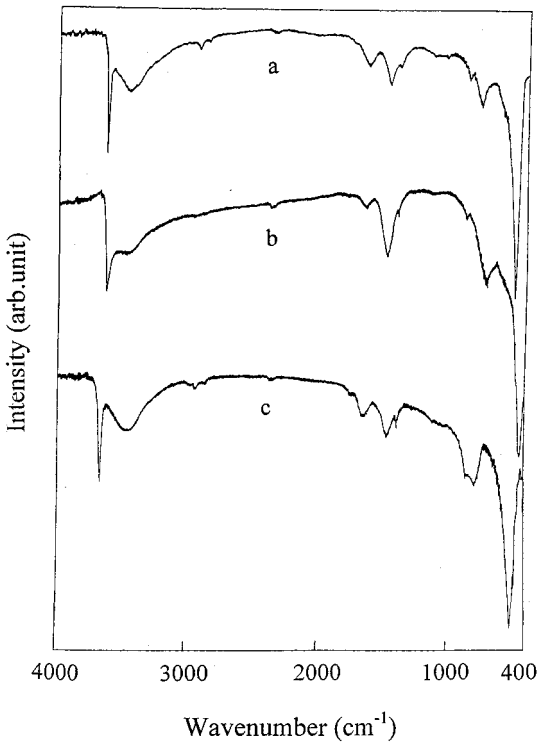

Figure 3. IR spectra at room temperature for (a) $Sr_3Cr_2(OH)_{12}$, (b) $Sr_3Fe_2(OH)_{12}$, and (c) $Sr_3Al_2(OH)_{12}$.

The lower temperature (e.g., 240 °C) synthesis of the single-phase nanocrystalline $Sr_3Cr_2(OH)_{12}$ benefitted from the high reactivity of the reactants employed in our hydrothermal system. As shown in Table 1, when the starting materials have low reactivities, such as the oxides Sr_2CrO_4 and $SrCrO_2$,[5] high temperature (e.g., 400 °C) and pressure (e.g., 1200 bar) hydrothermal condi-

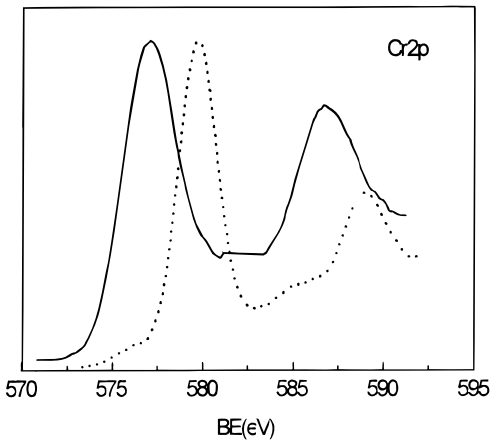

Figure 4. XPS of Cr2p for $Sr_3Cr_2(OH)_{12}$ (solid line) and mixture of $SrCrO_4$ and $SrCO_3$ (dash line). Binding energies of $Cr2p_{3/2}$ and $Cr2p_{1/2}$ for $Sr_3Cr_2(OH)_{12}$ are 577.1 and 585.3 eV, respectively, whereas binding energies of $Cr2p_{3/2}$ and $Cr2p_{1/2}$ for the mixture ($SrCrO_4$) systematically shifted 2.4 eV toward higher binding energies, showing valence variation from Cr-(III) to Cr(VI).

Table 1. Comparison of the Hydrothermal Conditions for Crystallization of Hydrogarnets $Sr_3M_2(OH)_{12}$ (M = Cr, Fe, and Al)

reactants	cryst temp (°C)	reaction pressure (bar)	ref
$Sr_3Cr_2(OH)_{12}$			
$Sr(OH)_2$, $Cr(NO_3)_3$, NaOH	240	autogenous	this work
Sr_2CrO_4, $SrCrO_2$, H_2O	400	1200	8
$Sr_3Fe_2(OH)_{12}$			
$Sr(OH)_2$, $Fe(NO_3)_3$, NaOH	240	autogenous	this work
$Sr_3Fe_2O_{7-x}$, NaOH	450	1000	8
$Sr_3Al_2(OH)_{12}$			
$Sr(OH)_2$, $Al(OH)_3$, NaOH	240	autogenous	this work
$Sr_3Al_2O_6$	400	1500	8

tions are required for the crystallization of the hydrogarnets. This implies that the solubilities as well as the reactivities of the starting materials determine the purity of hydrogarnet phases and the crystallization temperatures. Similarly, in other hydrothermal systems,[19] soluble precursors were usually employed for eliminating impurities; when precursors with low solubilities were used, stirring-assisted dissolution was needed for speeding up the formation of the single-phase products.

In Sr−Fe hydrothermal systems with $Fe(NO_3)_3 \cdot 9H_2O$ as the starting Fe source, a brown $Fe(OH)_3$ slurry was initially formed in the presence of NaOH.[20] This slurry has some solubility in basic conditions. The crystallinity and formation of the hydrogarnet phase can be increased by increasing the molar ratio of Sr/Fe near to 1.5. Figure 5a shows the XRD pattern for single phase $Sr_3Fe_2(OH)_{12}$. This phase is also cubic (*Ia*3*d*). The corresponding IR spectrum is given in Figure 3b. The sharp band at ca. 3600 cm^{-1} is assigned, as before, to the hydroxyl groups in the hydrogarnet lattice. The absorption bands at ca. 3450 and 1600 cm^{-1} come from the stretching and bending vibrations of adsorbed water, respectively. Under experimental conditions, such as filling capacity, initial concentrations and pH, similar to those for the synthesis of $Sr_3Cr_2(OH)_{12}$, rounded

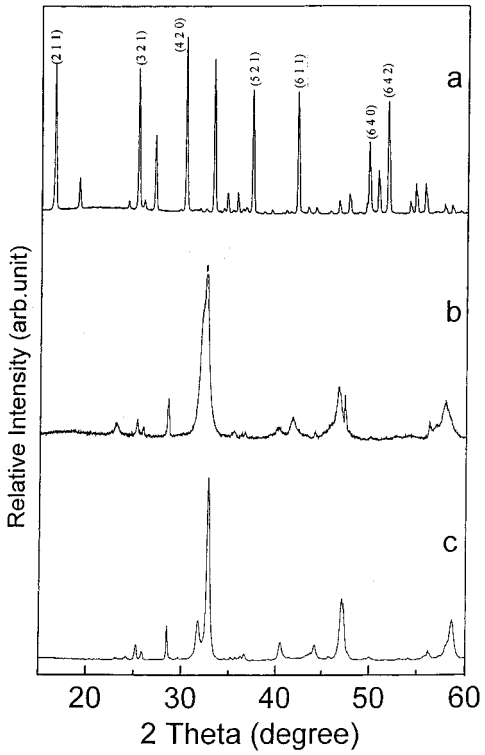

Figure 5. XRD patterns for (a) $Sr_3Fe_2(OH)_{12}$, (b) the sample obtained by decomposition of Sr−Fe hydrogarnet in DTA-TG measurement at 750 °C in flowing N_2, and (c) the sample produced by heating Sr−Fe hydrogarnet at 1150 °C in O_2.

particles of $Sr_3Fe_2(OH)_{12}$ with an average grain size of ca. 4.0 μm were obtained, as seen in the TEM photograph in Figure 2b. However, lower input molalities of Fe species (<0.17 mol/kg), lower pH values (<10), and greater deviation of molar ratio of Sr/Fe (e.g., 1 or 2) from the ideal Sr/Fe, 1.5 were found to prevent the crystallization of single phase $Sr_3Fe_2(OH)_{12}$. A hexagonal ferrite $SrFe_{12}O_{19}$ was reported[20−22] to form in a system with a small molar ratio of Sr/Fe, 0.083, and pH, ca. 12.

The formation reaction of $Sr_3Al_2(OH)_{12}$, in comparison with the syntheses of $Sr_3Cr_2(OH)_{12}$ and $Sr_3Fe_2(OH)_{12}$, could take place at the presence of a low concentration of OH^-, e.g., pH = 7−8, due to sufficient solubility of the input Al species in basic systems. In basic systems, the solubility of $Al(OH)_3$ is greatly larger than those of $Cr(OH)_3$ and $Fe(OH)_3$, as deduced from their acidic constants,[23] e.g., $Al(OH)_3$ (4.0×10^{-13}) ≫ $Cr(OH)_3$ (3.2×10^{-16}) (the acidic constant of slurry $Fe(OH)_3$ is extremely small and not given here for its alkalinity in basic systems). High solubilities of the ionic species favor a large amount of hydrated ions releasing for participation in the homogeneous formation reaction; this also eliminates the chance for the occurrence of impurities. On the other hand, highly crystalline $Sr_3Al_2(OH)_{12}$ can be formed in wider ranges of input concentrations, e.g., input molality of Al species, 0.10−0.17 mol/kg, and molar ratios, e.g., Sr/Al, 0.5−2. Figure 6a shows XRD pattern for single-phase $Sr_3Al_2(OH)_{12}$.

(19) Lenka, M. M.; Riman, R. E. *Chem. Mater.* **1995**, *7*, 18.
(20) Lin, C. H.; Shih, Z. W.; Chin, T. S.; Wang, M. L.; Yu, Y. C. *IEEE Trans. Magn.* **1990**, *26*, 15.
(21) Lee, K. H.; Lee, B. H.; Kim, S. K. *Yoop Hakhoechi* **1987**, *24*, 17.
(22) Ataie, A.; Ham's, I. R.; Ponton, C. B. *Br. Ceram. Proc.* **1994**, *52*, 273.
(23) Komal, N. L. *Principles of Analytic Chemistry*; Hkar'Kovskobo University: 1955.

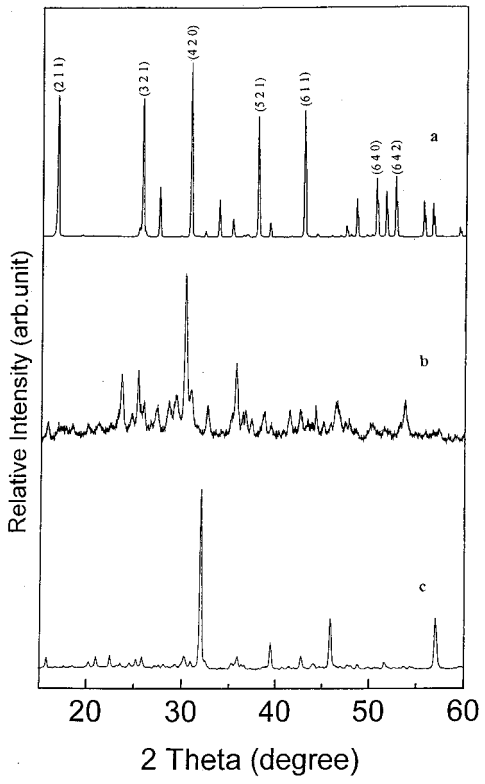

Figure 6. XRD patterns for (a) $Sr_3Al_2(OH)_{12}$, (b) $Sr_3Al_2O_6 \cdot H_2O$, produced by sintering $Sr_3Al_2(OH)_{12}$ at 400 °C in air, and (c) $Sr_3Al_2O_6$, by sintering $Sr_3Al_2(OH)_{12}$ at 600 °C in air.

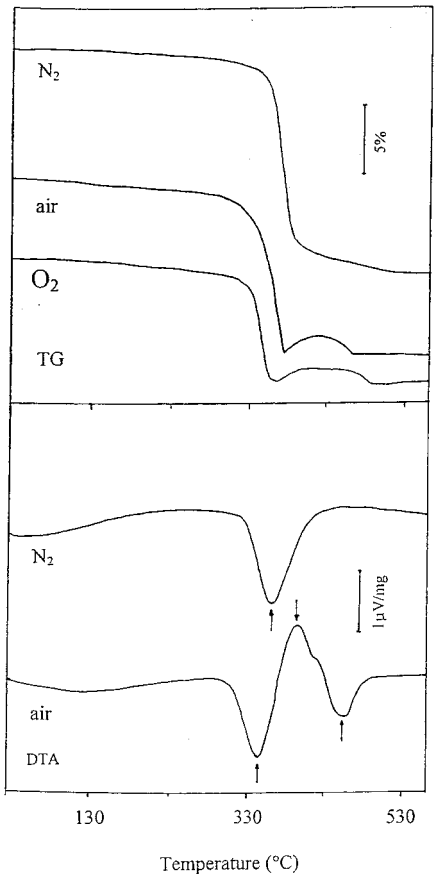

Figure 7. DTA-TG curves for $Sr_3Cr_2(OH)_{12}$ in air, O_2, and N_2.

This phase is also cubic. In the corresponding IR spectrum in Figure 3c, the absorption band at ca. 3600 cm^{-1} from OH^- stretching vibration of the lattice −OH in hydrogarnet, and the bands at ca. 3450 and 1600 cm^{-1} from OH^- stretching and bending vibrations in adsorbed water were also observed. Experimental conditions similar to those used for the syntheses of Sr−Cr and Sr−Fe hydrogarnets produced powders with an average grain size, ca. 4.0 μm, as shown in the TEM photograph in Figure 2c. It is clear that high solubility of the starting materials promotes the growth rate of the particles as well as the crystallinity of the final products.

2. Structural Stability and Thermal Decomposition Behaviors of the Hydrogarnets. Figure 7 shows DTA-TG curves for $Sr_3Cr_2(OH)_{12}$ in air, O_2, and N_2. In air, two endothermic peaks at ca. 340 and 445 °C with weight losses and an exothermic peak at ca. 355 °C with weight gain were observed. According to the formula of the hydrogarnet, complete dissipation of water by condensation of the lattice hydroxyl groups in $Sr_3Cr_2(OH)_{12}$ would result in a total weight loss of 18.92%. It is reasonable that the endothermic peak around 340 °C with a sharp weight loss of 12.84% corresponds to a fast dehydration of ca. 4 H_2O molecules (the expected weight loss of 4 H_2O in $Sr_3Cr_2(OH)_{12}$ is 12.61%), accompanied by collapse of the hydrogarnet lattice. Another endothermic peak at ca. 445 °C is also ascribed to the loss of the remaining hydroxyl groups, and this weight loss was partially counteracted by the weight gain at ca. 355 °C due to oxidation of Cr(III) ions.

With further heating $Sr_3Cr_2(OH)_{12}$ from 480 to 1150 °C, the DTA-TG measurement showed no obvious thermal effects. This eliminates the possibility for the formation of $SrCO_3$ at ca. 355 °C, because no peak or weight variation corresponding to the decomposition of $SrCO_3$ at ca. 600 °C was found. The cooling curves of DTA-TG from 1150 °C to room temperature also showed no peaks, especially during the temperature interval where a "bump" appeared in the TG heating curve in air. These results show an irreversible thermodynamic process, e.g., the high-temperature decomposition product on annealing $Sr_3Cr_2(OH)_{12}$ in air is stable. Figure 1c is the XRD pattern for the decomposition product after sintering nanocrystalline $Sr_3Cr_2(OH)_{12}$ at 600 °C in air for 5 h. Analysis of the data indicated that the air-decomposed products are $SrCrO_4$ and SrO (the formation of $SrCO_3$ observed by XRD was due to gradually trapping CO_2 from the air at room temperature).

It is known that gaseous H_2O dissipated can be removed immediately by flowing O_2 during the DTA-TG measurements, and the effects from the dissipated water on the decomposition processes are effectively avoided. However, we did observe a similar weight gain in O_2 to that in air, as seen in Figure 7. This shows that the weight gain at ca. 355 °C is not due to the formation of $Sr(OH)_2$. In comparison with the TG curve measured in air, the Sr−Cr hydrogarnet in O_2 produced a slightly smaller sharp weight loss (9.12%). This shows that the oxygen concentration in the atmosphere is an important factor for the oxidation of Cr(III) ions.

The oxidation process can be prevented by flowing N_2. As shown in Figure 7, in N_2 the TG-DTA of $Sr_3Cr_2(OH)_{12}$ does not show any exothermic peak or a weight gain. The sharp weight loss at ca. 382 °C is 14.50%, slightly larger than that measured in air (12.84%). The reason

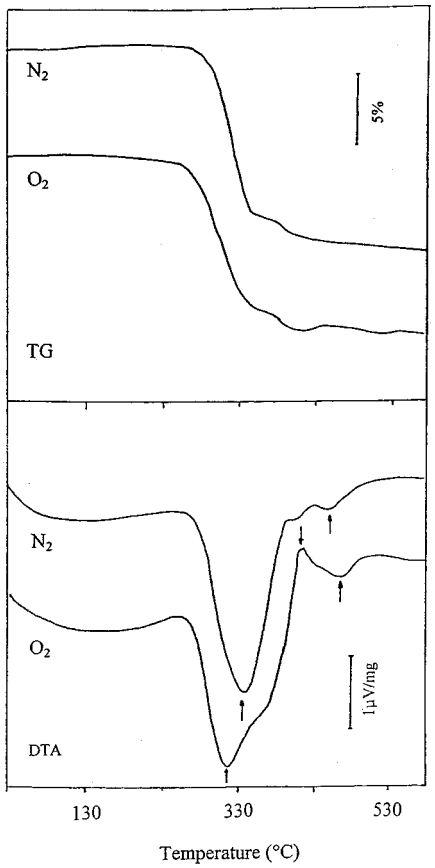

Figure 8. DTA-TG curves for $Sr_3Fe_2(OH)_{12}$ in O_2 and N_2.

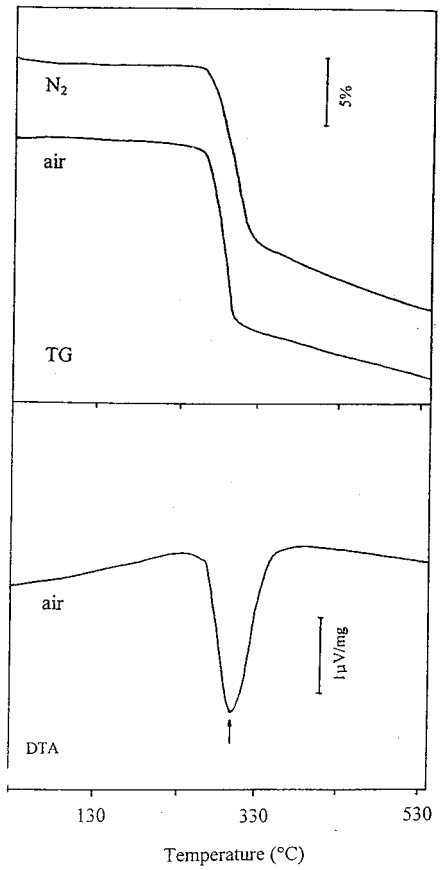

Figure 9. DTA-TG curves for $Sr_3Al_2(OH)_{12}$ in air and N_2.

for the differences in weight losses in O_2, air, and N_2 is possibly due to differences in the oxidation weight gain for Cr(III) in O_2 or air. The slow weight loss process following the sharp one is ascribed to slow dehydration of the remaining OH^- ions in the decomposition product. The freshly decomposed product of $Sr_3Cr_2(OH)_{12}$ at 750 °C in N_2 was also examined at room temperature by XRD (Figure 1b). A poorly crystalline decomposition product of $Sr_4Cr_2O_8$ was obtained; it can be indexed in rhombohedral symmetry, *R*3*m*, and is an analogue of $Ba_3(PO_4)_2$;[24] this phase is also isostructural with $Sr_{3.63\ 0.33}(CrO_4)_{1.33}(CrO_4)_{0.67}$, as prepared by Hartl et al.[25] from Sr−Cr−O solid-state system. Big dispersed diffraction peaks suggest there coexist certain amorphous phases.

The valence state of Cr ions in the air decomposed product of $Sr_3Cr_2(OH)_{12}$ was determined by surface XPS, as seen in Figure 4 (dash line). The peak positions of $Cr2p_{3/2}$ and $Cr2p_{1/2}$ in the decomposed product by sintering $Sr_3Cr_2(OH)_{12}$ in air at 600 °C has systematically shifted 2.4 eV toward a higher binding energy in comparison with those (solid line) in $Sr_3Cr_2(OH)_{12}$, accompanied with an obvious decrease of the half-height width. This confirms the presence of Cr(VI) ions. Theoretically, complete oxidation from Cr(III) to Cr(VI) for each mole of $Sr_3Cr_2(OH)_{12}$ requires 3 mol of oxygen atoms, which corresponds to a weight variation, 8.4%. Experimentally, the oxygen amount involved in the oxidation reaction, corresponding to the weight gain in O_2, is quantitatively obtained by comparing the masses of the two decomposition products in O_2 and N_2, respectively. For example, at 530 °C, the weight loss in O_2 is 9.4%, whereas in N_2 it is 16.2%; the weight difference is 6.8%, close to the calculated value (8.4%).

Figure 8 shows the DTA-TG curves for $Sr_3Fe_2(OH)_{12}$. In a flowing O_2, two endothermic peaks at ca. 320 and 440 °C, with weight losses, and one exothermic peak at ca. 410 °C, with a small weight gain, were observed. The sum of the weight losses at ca. 320 °C was 12.52%, which is ascribed to the loss of 4 H_2O molecules in $Sr_3Fe_2(OH)_{12}$ (the ideal weight loss for 4 H_2O is 12.44%). These two dehydration processes are completed in a wide temperature range, 246−403 °C in O_2. This suggests that in the $Sr_3Fe_2(OH)_{12}$ lattice, Fe(III) ions are in more complex coordination states than the Cr(III) ions in $Sr_3Cr_2(OH)_{12}$. XRD and IR analyses on the decomposed product of $Sr_3Fe_2(OH)_{12}$ in O_2 showed that the weight gain at ca. 410 °C comes from the oxidation of Fe(III) rather than the formation of $SrCO_3$ or $Sr(OH)_2$.

For each mole of $Sr_3Fe_2(OH)_{12}$, complete oxidation from Fe(III) to Fe(IV) theoretically requires 1 mol of oxygen atoms, which corresponds to a weight gain of 2.8%. From the TG curves of $Sr_3Fe_2(OH)_{12}$ in O_2 and N_2, we obtained a mass difference of 1.8% (at 530 °C), smaller than the theoretical value (2.8%), suggesting partial oxidation of Fe(III) ions. From the DTA curves of $Sr_3Fe_2(OH)_{12}$ in O_2 (Figure 8), we confirmed that the dehydration process, loss of four water molecules (endothermic peak at 310 °C), was followed by an oxidation process for Fe(III) (exdothermic peak at 350 °C). In N_2, no weight gain due to oxidation was observed. The decomposition products of $Sr_3Fe_2(OH)_{12}$ in N_2 and O_2 were unknown. The XRD patterns in Figure 5b,c do not correspond to $Sr_3Fe_2O_{7-x}$, or the perovskite $SrFeO_{3-\delta}$

(24) McLune, W. F., Ed. *Powder Diffraction File: Inorganic Phases*; JCPDS International Centre for Powder Diffraction Data: Swarthmore, PA, Card No. 25-28, 1989.

(25) Hartl, K.; Braungard, R., *Z. Naturforsch. B*: *Anorg. Chem., Org. Chem*. **1978**, *33B*, 952.

Table 2. ^{57}Fe Mossbauer Parameters of $Sr_3Fe_2(OH)_{12}$ and Its Air Decomposition Product at 750 °C, Recorded at Room Temperature

sample[a]	site	I.S. (mm/s)[a]	Q.S. (mm/s)[a]	H_{in} (kOe)[a]	fwhm (mm/s)[a]	intensity (%)[a]
A	Fe(1)	0.369 ± 0.004	0.201 ± 0.008	516.0 ± 0.2	0.132 ± 0.004	48.0
	Fe(2)	0.351 ± 0.004	0.232 ± 0.004			52.0
B	Fe(1)	0.362 ± 0.007	0.200 ± 0.009	516.9 ± 0.5	0.131 ± 0.006	24.0
	Fe(2)	0.234 ± 0.006	0.640 ± 0.008		0.196 ± 0.004	33.7
	Fe(3)	0.105 ± 0.004	0.246 ± 0.004			42.3

[a] Note: A denotes $Sr_3Fe_2(OH)_{12}$; B, decomposition product of $Sr_3Fe_2(OH)_{12}$ at 750 °C in air. I. S., isomer shift (vs α-Fe), Q. S., quadrupole splitting, H_{in}, hyperfine field, and fwhm, half-height width; intensity corresponds to integrated area of the Mossbauer spectrum.

as reported by Gallagher and others[26,27] by calcination of $SrCO_3$ and Fe_2O_3 in air, or under high oxygen pressure.

Figure 9 shows DTA-TG curves for $Sr_3Al_2(OH)_{12}$ in air and N_2. The TG curves in air and N_2 show a fast dehydration process at around 262 °C and a gradual one above 326 °C. The fast process corresponds to a weight loss of 13.82%, exactly the same as that expected for the loss for 4 H_2O molecules per formula of $Sr_3Al_2(OH)_{12}$. The gradual weight loss process is ascribed to the slow dehydration of the remaining OH^-. The dehydration processes for $Sr_3Al_2(OH)_{12}$ in air and N_2 were similar to those for $Sr_3Cr_2(OH)_{12}$ and $Sr_3Fe_2(OH)_{12}$ in N_2. This clearly demonstrates the effects of the atmospheres and the valence variations of the framework ions on the decomposition processes. Figure 6b,c show the XRD patterns for the decomposition products by sintering $Sr_3Al_2(OH)_{12}$ at 400 and 600 °C in air, respectively. Structural analyses suggested the following decomposition processes for $Sr_3Al_2(OH)_{12}$ in air:

$$Sr_3Al_2(OH)_{12} \rightarrow Sr_3Al_2O_6 \cdot 2H_2O + 4H_2O \qquad 262-326\ °C$$

$$Sr_3Al_2O_6 \cdot 2H_2O \rightarrow Sr_3Al_2O_6 \cdot H_2O + H_2O \qquad 400\ °C$$

$$Sr_3Al_2O_6 \cdot H_2O \rightarrow Sr_3Al_2O_6 + H_2O \qquad >600\ °C$$

It is interesting to note that $Sr_3Al_2O_6$ can be readily obtained from $Sr_3Al_2(OH)_{12}$ as a precursor at 600 °C, whereas in a solid-state reaction, $Sr_3Al_2O_6$ can be formed only at ca. 1600 °C with several intermediate grinding steps.[28] Alternatively, under a high temperature and pressure hydrothermal condition, $Sr_3Al_2O_6$ will be transformed to hydrogarnet $Sr_3Al_2(OH)_{12}$ (Table 1). The decomposition studies of the Sr−Al, Sr−Cr, and Sr−Fe hydrogarnets indicate that the valence variations of the garnet framework ions are closely correlated to the thermal decomposition processes and resulting structures in the final decomposition products of the hydrogarnets.

The structure of the general binary hydrogarnet $A_3^{II}B_2^{III}(OH)_{12}$ is constructed from alternating blocks of $B(OH)_6$ octahedra linked together by A^{2+} ions which occupy the centers of dodecahedra.[29] Each hydroxyl group is connected to two dodecahedra and one octahedron. This network creates hydroxyl tetrahedra, which

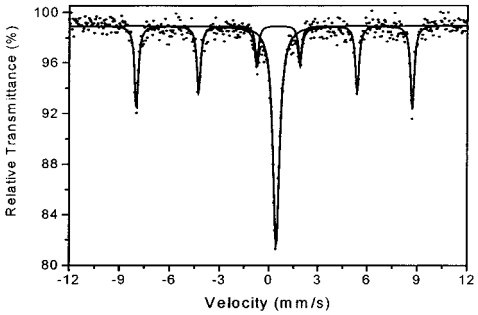

Figure 10. ^{57}Fe Mossbauer spectrum for $Sr_3Fe_2(OH)_{12}$ at room temperature (with a ^{57}Co/Rh radiation source).

are empty at the center. The hydroxyl tetrahedron are isolated. The formula for the hydrogarnets can be written $\{A(OH)_{8/3}\}_3 \cdot \{B(OH)_2\}_2$.[5] The effective number of the hydroxyl groups of A dedocahedra per formula is eight. Thus, the hydrogarnets show marked covalent character. In Sr-based hydrogarnets, the eight hydroxyl groups bonded to Sr dodecahedra, in comparison with those bonded in adjacent transition-metal octahedra, may be easily removed as the temperature increases, corresponding to the loss of four water molecules. As the dehydration processes and the oxidation of transition-metal ions in the octahedra begin to take place, they have opposite effects on weight changes in the TG measurements. However, the dehydration process in N_2 may not be affected by oxidation.

The initial decomposition temperatures for Sr−Fe, Sr−Al, and Sr−Cr hydrogarnets in N_2 are 252.1, 261.7, and 341.1 °C, respectively. This indicates a sequence of the structural stability of Sr based hydrogarnets: $Sr_3Fe_2(OH)_{12} < Sr_3Al_2(OH)_{12} < Sr_3Cr_2(OH)_{12}$.

3. ^{57}Fe Mossbauer Effects in $Sr_3Fe_2(OH)_{12}$ and Its Air Decomposition Product. Figure 10 shows ^{57}Fe experimental Mossbauer spectrum of $Sr_3Fe_2(OH)_{12}$ at room temperature, and Table 2 lists corresponding Mossbauer parameters. The experimental data can be resolved into a six-line and a single-line spectra, respectively, suggesting that in the lattice of $Sr_3Fe_2(OH)_{12}$, Fe ions occupy two different sites, denoted as Fe(1) and Fe(2). From the isomer shift (I.S.) values (vs α-Fe) in Table 2, it can be concluded that all Fe ions in $Sr_3Fe_2(OH)_{12}$ are trivalent. The quadrupole splitting (Q.S.) values of the Fe(1)-site ions, corresponding to a six-line Mossbauer spectrum, are less than 1.0 mm/s. This indicates that, the Fe(1)-site ion has a distorted octahedral coordination. A study[30] of the ^{57}Fe Mossbauer spectrum of $Y_3Fe_5O_{12}$ showed that at room temperature the experimental spectrum consisted of two sets of six-line spectra; the internal fields of the Fe ions at the centers of octahedra and tetrahedra were ca. 490 and

(26) (a) Gallagher, P. K.; MacChesney, J. B.; Buchanan, D. N. E. *J. Chem. Phys.* **1964**, *41*, 2429. (b) **1966**, *45*, 2466 and references therein.

(27) Bocques, A. E.; Fujimori, A.; Mizokawa, T. *Phys. Rev. B* **1992**, *45*, 1561.

(28) McLune, W. F., Ed. *Powder Diffraction File: Inorganic Phases*; JCPDS International Centre for Powder Diffraction Data: Swarthmore, PA, Card No. 24-1187, 1989.

(29) Weiss, P. R.; Grandjean, D.; Pavin, J. L. *Acta Crystallogr.* **1964**, *17*, 1329.

(30) Belogurov, V. N.; Bilinkin, V. A., *Phys. Status Solidi A* **1981**, *63*, 45.

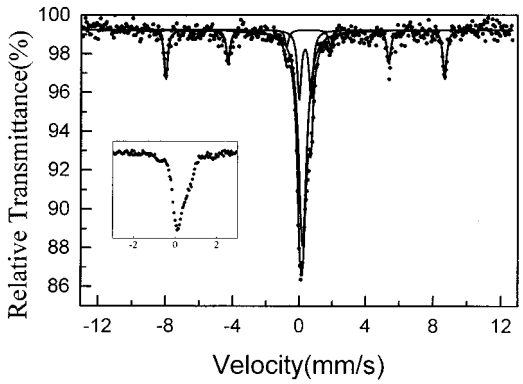

Figure 11. ^{57}Fe Mossbauer spectrum recorded at room temperature for the decomposition product of $Sr_3Fe_2(OH)_{12}$ at 750 °C in air (with a ^{57}Co/Rh radiation source). Insert shows the asymmetry of the paramagnetic spectrum.

393.7 KOe, respectively, and Q.S. $\neq 0$. However, in the hydrogarnet lattice, the centers of the tetrahedra are empty due to the formation of point vacancies, and thus the Fe ions in tetrahedra were not observed in our case. In addition, the nearly equal integrated intensities of the six-line and single-line spectra indicated that the nearly equal numbers of the Fe ions are distributed at the Fe(1) and Fe(2) sites. It is clear that the Fe(2)-site ions, associated with the single-line spectrum are coordinated with hydroxyl groups in highly symmetric octahedra, where more symmetrical electric fields around the nuclei of Fe(2)-site ions are produced. Therefore, two kinds of $Fe(OH)_6$ octahedron in $Sr_3Fe_2(OH)_{12}$, could be concluded. The local distortion due to the presence of Fe(1) ions in $Sr_3Fe_2(OH)_{12}$ is consistent with the lowest thermal stability of $Sr_3Fe_2(OH)_{12}$ in the three Sr-based hydrogarnets studied.

The decomposition product of $Sr_3Fe_2(OH)_{12}$ is of great interest because there may exist an unusual oxidation of Fe(III) to Fe(IV) by air or O_2. Figure 11 is the ^{57}Fe Mossbauer spectrum recorded at room temperature for the air decomposed product of $Sr_3Fe_2(OH)_{12}$ at 750 °C. Comparison of the data in Figure 11 with that in Figure 10 shows that the states of Fe ions change dramatically after sintering $Sr_3Fe_2(OH)_{12}$ in air. In addition to a six-line spectrum, a broad paramagnetic component was observed, insert clearly indicates its asymmetry. The experimental data can be resolved into a six-line, a doublet, and a single-line spectrum, clearly suggesting that there exist three distinctive states of Fe ions in the air decomposition product of $Sr_3Fe_2(OH)_{12}$ (denoted as Fe(1), Fe(2), and Fe(3), respectively). The assignments and corresponding Mossbauer parameters are listed in Table 2. According to the I.S. values of Fe(IV) and Fe(III) in literature,[26,31] it can be concluded that all Fe ions at Fe(1) site (associated with the six-line spectrum) and Fe(2) site (associated with the doublet spectrum) are trivalent; the Fe(2)-site ions have a larger Q.S. value, indicating that the coordination polyhedra of the Fe(2)-site ions have larger distortion. Fe(3)-site ions, associated with the single-line spectrum, correspond to the high-spin Fe(IV). The largest integrated intensity of the single line spectrum (42.3%) gives an evidence for the existence of a pronounced amount of Fe(IV) ions in the decomposition product arising from the oxidation of Fe(III) to Fe(IV) by air (or O_2) during the sintering procedures.

Conclusions

Hydrogarnets $Sr_3M_2(OH)_{12}$ (M = Cr, Fe, and Al) were hydrothermally prepared under relatively mild conditions. In the hydrothermal systems of Sr-based hydrogarnets, high solubility of initial reactants and concentration of mineralizer (OH^-) considerably lower the crystallization temperature and enhance the crystallinity of the resulting hydrogarnets. All samples of Sr-based hydrogarnets underwent fast dehydration processes by dissipation of the nearest hydroxyl groups of Sr dodecahedra in N_2. In air or O_2, such dehydration processes were accompanied with oxidation of Cr(III) and Fe(III) ions in Sr−Cr and Sr−Fe hydrogarnets. $Sr_3Al_2(OH)_{12}$, synthesized from the hydrothermal system, could be used as a precursor for preparing $Sr_3Al_2O_6$ at ca. 600 °C (1600 °C was needed in a conventional solid-state reaction). Valence variations of framework ions, such as Cr(III) and Fe(III), directly determined the types and compositions of the final decomposition products. Two different symmetries of $Fe(OH)_6$ octahedra in the Sr−Fe hydrogarnet as well as its air oxidation were detected by Mossbauer spectroscopy; the lowest thermal stability of $Sr_3Fe_2(OH)_{12}$ was attributed to the distortion of one of the $Fe(OH)_6$ octahedra.

Acknowledgment. This work was financially supported by the NSFC through the National Outstanding Youth Science Fund and the State Education Commission through the Excellent Talent Plan (S.F). G.L. thanks Dr. Dapeng Xu, Physics Department for some reproducible work in TG-DTA measurements and Prof. Xizhang Cao and Xingqiao Wang, Chemistry Department, Jilin University, for discussion.

CM9702373

(31) Nakano, M.; Okita, T.; Nakayama, N.; Bando, Y.; Takeda, Y.; Yamamoto, O.; Goodenough, J. B. *J. Solid State Chem.* **1988**, *73*, 140.